Coacervation and aggregation in lysozyme/alginate mixtures

Asna Vakeri, Adeline Boire, Joelle Davy, Pascaline Hamon, Antoine Bouchoux, Said Bouhallab, Denis Renard

Food Hydrocolloids 156 (2024) 110359

Contents lists available at ScienceDirect

Food Hydrocolloids

journal homepage: www.elsevier.com/locate/foodhyd

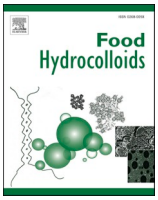

Coacervation and aggregation in lysozyme/alginate mixtures

Asna Vakeri [a,*], Adeline Boire [a], Joelle Davy [a], Pascaline Hamon [b], Antoine Bouchoux [c], Saïd Bouhallab [b], Denis Renard [a]

[a] UR 1268 Biopolymères Interactions Assemblages, INRAE, 44316, Nantes, France
[b] INRAE, Institut Agro, UMR1253 STLO, F-35042, Rennes, France
[c] TBI, Université de Toulouse, CNRS, INRAE, INSA, Toulouse, France

ARTICLE INFO

Keywords:
Aggregation
Complex coacervation
Ionic strength
Phase diagram
Droplet millifluidic

ABSTRACT

Upon electrostatic interaction, the mixture of oppositely charged macromolecules separates into a macromolecule-rich dense phase coexisting with a diluted phase. The associative interaction proceeds through either liquid-liquid phase separation (LLPS) forming complex coacervates or liquid-solid phase separation (LSPS) forming aggregates. We here investigate the assembly of the basic protein lysozyme (LYS) with the negatively charged polysaccharide alginate (ALG) at pH 7 in different conditions of mixing ratios, total concentration, and ionic strength using a droplet-based millifluidic device. Aggregation and coacervation are observed in this system by changing the salt concentration. A 3D phase diagram, with concentration of salt, lysozyme, and alginate as 3D coordinates, gives a thorough description of monophasic, liquid-solid, and liquid-liquid phase separation areas, and the regions where both solid and liquid phases coexist. The thermodynamic aspects behind these two kinds of complex formation are investigated using isothermal titration calorimetry (ITC). Aggregation is associated with a strong affinity between LYS and ALG, with a 100 LYS: 1 ALG stoichiometry ratio, whereas a decreased binding affinity between the two biopolymers leads to coacervation.

1. Introduction

When oppositely charged polyelectrolytes (e.g. PEs and polysaccharides) and colloids (e.g. micelles and proteins) interact, entropic and/or electrostatic effects lead to either liquid-liquid (LLPS) or liquid-solid (LSPS) phase separation. The liquid-liquid phase separation is called 'complex coacervation', and results in the formation of a dense polymer-rich phase along with a supernatant (Pathak, Priyadarshini, Rawat, & Bohidar, 2017). This phenomenon is now popular due to its applications including personal care (Turgeon, Schmitt, & Sanchez, 2007), biomaterials (Blocher & Perry, 2017; Sinha et al., 2023), protein purification (Romanini, Braia, Angarten, Loh, & Picó, 2007), and food science (Schmitt & Turgeon, 2011). In contrast, aggregation, which is the other possible phase separation (LSPS), has always represented a problem by introducing inhomogeneities, irreversibility, and irreproducible kinetics. Therefore, understanding the dominant factors driving the formation of aggregates or precipitates is important to control outcomes (Comert, Malanowski, Azarikia, & Dubin, 2016).

In terms of morphology, complexation appears in the form of a fluid phase (coacervate droplets of homogeneous aspect) or solid aggregates. The origin of these two distinct assemblies is still largely misunderstood, judging by the absence of a generic framework capable of predicting the physical state of polyelectrolyte complexes. Concerning the thermodynamic aspects, it is accepted that complexation is always favoured by the entropic gain related to the release of counter ions. However, nothing is as certain from the point of view of enthalpy, where complexation can be both endothermic and exothermic, depending on the systems considered. Previous works suggest that aggregate forms when the interaction between the macromolecules is strong, while coacervation happens at lower interaction strength (Ghosh, Bose, & Tang, 2021). In that respect, increasing salt concentration (Zheng et al., 2022; Liu, Momani, Winter, & Perry, 2017), adding urea (Perry et al., 2015), or increasing temperature (Nigen, Croguennec, Renard, & Bouhallab, 2007) weaken the interaction between the macromolecules causing a change in the obtained complex from solid aggregates to liquid coacervates. When it comes to systems involving proteins, charge distribution plays an important role in the involved interactions (Kurut, Persson, Åkesson, Forsman, & Lund, 2012; Persson & Lund, 2009). For polyelectrolytes,

* Corresponding author. Unité Biopolymères Interactions Assemblages, INRAE Pays de la Loire, 3 Impasse Yvette Cauchois, La Géraudière, CS 71627, 44316, Nantes, Cedex 3, France.
E-mail address: asna.vakeri@inrae.fr (A. Vakeri).

https://doi.org/10.1016/j.foodhyd.2024.110359
Received 13 February 2024; Received in revised form 14 May 2024; Accepted 25 June 2024
Available online 27 June 2024

the surface charge density is of prior importance. High-charged polyelectrolytes are prone to aggregation whereas weakly-charged polyelectrolytes form coacervates (Schmidt, Cousin, Huchon, Boué, & Axelos, 2009). In addition, the flexibility and stiffness of the polymers also play a crucial role in determining the type of phase separation (Pathak et al., 2017). As an example, the overall and local charge densities of pectin (random vs blockiness charges distribution) have an impact on the size and distribution of β-lactoglobulin clusters within the primary protein-polysaccharide complexes. Moreover, depending on the spatial arrangement of the primary complexes, the resulting structure can be either a complex coacervate or a precipitate (Xu et al., 2018). Comert and co-workers propose that coacervation and precipitation are intrinsically different phenomena, affected by different factors (Comert et al., 2016). Today, to our knowledge, there is no general description of those factors, nor is there any unified mechanism to define the aggregation and coacervation pathways.

In general, the charge and structure of the (bio)-polymers are the key factors determining interaction strength. Ionic strength is a parameter of prior importance as it can screen the charges and affect the strength of interaction. In this work, we tune the interaction strength between the protein lysozyme (LYS) and the negatively charged polysaccharide alginate (ALG) at pH 7 b y the addition of monovalent salt, along with analysing the complex formation in different mixing ratios and total macromolecular concentration. LYS is a basic protein possessing a homogenous surface distribution of positive charge at pH 7 with less exposed negative domains (Ainis et al., 2019). ALG is a negatively charged linear polysaccharide composed of (1/4)-β-D-mannuronopyranosyl and (1/4)-α-L-guluronopyranosyl units (Harnsilawat, Pongsawatmanit, & McClements, 2006). A fixed pH of 7 was chosen here as both of our biopolymers carry opposite charges. This work is not intended to look at the effect of pH on the interaction of the biopolymers but focuses on the effect of ionic strength.

Studies have been carried out previously on the LYS/ALG mixture as self-assembling electrostatic complexes (Fuenzalida et al., 2016). Even though the couple has been studied extensively for its potential application as antibacterial films (Wu, Huang, et al., 2018), drug delivery vehicles (Wu, Li, Shen, Yuan, & Hu, 2018), and in LYS recovery technique (Sun, Xiao, & Huang, 2019), studies on this couple in the context of the propensity to form aggregate and coacervate have not been explored. In this study, we highlight the conditions of interactions and phase separation in the LYS/ALG system by establishing a phase diagram using a homemade droplet-based millifluidic device (Amine, Boire, Davy, Marquis, & Renard, 2017, 2020). By starting with the analysis of the phase behaviour in different conditions of biopolymer concentration and added salt, we investigate the conditions leading to aggregation and coacervation in the couple. We then identify the thermodynamic parameters behind both phase separation pathways. To our knowledge, it is the first study that covers such a large range of experimental conditions thanks to droplets-based millifluidic enabling the identification of four areas in the phase diagram, monophasic, LLPS, LSPS, and coexistence of LLPS and LSPS. This thorough phase behaviour analysis could serve as a starting material to build new applications in the field of microencapsulation and drug delivery for instance.

2. Materials and methods

2.1. Materials

Commercially available ALG (SATALGINE S 60 NS, 157 000 g/mol) from Cargill and LYS (14 700 g/mol) from Roche Diagnostics GmbH (product number: 43092923) were used in all experiments. HEPES buffer was purchased from Sigma Aldrich (product number: 102479826). NaCl (CAS: 7647-14-5), NaOH (CAS: 1310-73-2), and HCl (CAS: 7647-01-0) used were from Sigma Aldrich. Sunflower seed oil from *Helianthus annuus* was purchased from Sigma Aldrich (CAS: 8001-21-6). MilliQ water was used for all experiments.

2.2. Biopolymers stocks dispersions

Both the LYS and ALG biopolymers were solubilized overnight in 10 mM HEPES buffer (pH 7, no added salt) under magnetic stirring. The dispersions were centrifuged (7378×*g* for 10 min) to remove insoluble residues and filtered further through a 0.2 μm cellulose acetate membrane (Sartorius, France).

The concentration of LYS was determined by UV absorption spectroscopy (Thermo Scientific Varioskan LUX Multi-Mode Microplate Reader). 3 μL of protein samples were drop-casted on the microplate (Thermo Scientific μDrop™ plate-ref: N12391) and the absorbance at 280 nm was measured. The concentration was calculated using the molar extinction coefficient value 2.4 L/g.cm (Ainis et al., 2019), and the path length value of 0.5 ± 0.02 mm. ALG concentration was determined by dry matter analysis.

2.3. Screening LYS-ALG interaction by droplet-based millifluidic device

The droplet-based millifluidic device was used for establishing the phase diagrams. This device has been previously developed and validated for screening phase diagrams. This setup has been found to have the advantages of small material consumption and fast generation of droplets (Amine et al., 2017, 2020). We here used the same setup to probe the interaction of LYS and ALG. The LYS and ALG stock solutions in the required concentrations were taken in two 2.5 mL glass syringes (Hamilton) and oil was taken in a 10 mL syringe placed on syringe pumps (Harvard Apparatus PHD 2000; France) with controlled flow rates. The flow rate of the oil continuous phase was fixed at 10 mL/h and the total flow rate of both the dispersion phases at 50 μL/min. Mixing of the dispersed phase took place inside a T-junction (thru-hole = 0.5 mm, swept volume = 0.57 μL, Upchurch Scientific®), and due to the co-flow geometry, the droplets flow out from the capillary (inner diameter = 0.53 mm, outer diameter = 0.66 mm, and length = 6.9 cm) along with the oil continuous phase. After production, droplets were passed through a serpentine channel (inner diameter = 1.42 mm, outer diameter = 3.14 mm, and length = 31 cm) for enhanced mixing inside the droplets. After production, the droplets took 3 min and 45 s to reach the observation zone with the chosen tube lengths. Image acquisition started once the droplets in the Tygon® tube connected to the serpentine channel reached the observation zone consisting of an open cell (made up of crosslinked PDMS moulded on a glass slide) in which the tube was held. Inside the cell, the pipe was immersed in 7 mL of ethylene glycol. The macro vision optical setup consisted of a camera, an objective, and 12 LEDs arranged circularly to obtain a dark field-like mode. The droplet composition was tuned by changing flow rates using a computer-assisted interface that controlled flow rates and time intervals. The LYS:ALG mixing ratios (mass ratios) tested were 0:1, 1:16, 1:8, 1:4, 1:2, 1:1, 2:1, 4:1, 8:1, 16:1, 1:0. A MATLAB script has been developed and used to analyse the mean grey level inside the droplet. The grey level was measured in the whole area inside the droplets leaving some portion close to the boundary. The correlation between turbidity and mean grey level was verified using TiO_2/water suspension. The grey level contributions from individual LYS and ALG were subtracted from the mean grey level values of each mixing ratio. Phase separation was observed in the mixture when the mean grey level was above a threshold value. This point (cloud point) was identified to correspond to a 50 % decrease in the transmitted light (Amine et al., 2017). This threshold grey level value is just an indication of phase separation, and it varies depending on the system and the conditions of biopolymer concentration and ionic strength. The grey level distribution histogram inside the droplet was obtained using Image J software (version 1.53k, developed by NIH).

The phase diagram was built by taking three parameters into account: mixing ratios of the biopolymers, total biopolymer concentration, and the NaCl concentration. LYS and ALG stock solutions at different concentrations ranging from 1 g/L to 10 g/L were prepared with varying amounts of added NaCl (10 mM–200 mM). The formation of aggregates

and coacervates at each point was confirmed with optical microscopy.

2.4. Isothermal titration calorimetry

LYS/ALG interactions were studied using ITC with a VP-ITC microcalorimeter (MicroCal VP-ITC, Malvern Panalytical, Malvern, UK) with sequential injections of ALG solution into LYS solution loaded into a sample cell having a volume of 1.425 mL. Titration experiments were performed at 25 °C under two different conditions of ionic strength corresponding to aggregation and coacervation. All dispersions prepared in 10 mM HEPES (with 0 or 75 mM NaCl added) at pH 7 were degassed under vacuum before the titration experiments. The reference cell was filled with 10 mM HEPES buffer and the sample cell was filled with LYS solution. LYS was titrated with 25 consecutive injections of 10 μL of ALG solution. The initial delay was set at 60 s and the stirring speed inside the sample cell was set at 300 rpm to ensure the homogeneity of the cell solution during the titration. The interval between injections was 200 s. Control experiments were carried out for each measurement by titrating the ALG solutions directly into 10 mM HEPES buffer containing the required concentration of NaCl. The signal associated with this reference injection is subtracted from the corresponding experimental signal. The point corresponding to the first injection is omitted before analysing the data since it is inaccurate. ITC data were fitted using the "one set of sites" fitting procedure of the MicroCal Origin ITC analysis software. From this non-linear least squares fit of calorimetric titration data, the parameters K (binding constant), ΔH_0 (enthalpy), and N (stoichiometry parameter) were determined directly. It must be noticed that the fitting model is more appropriate to describe the binding of small ligands in specific site(s) on larger host molecules. Nevertheless, as the obtained isotherms exhibited rather simple dominating single-phase profiles, this simplistic model was used as a first approximation to determine the interacting parameters for our systems. The salt conditions required to reach either aggregation or coacervation were chosen based on the results from the droplet millifluidic experiments.

2.5. Microscopy

All the mixtures were imaged under an inverted phase contrast microscope ((Olympus IX51) equipped with a camera (HAMAMATSU digital camera; C4742-95) and a phase contrast optical microscope (BX51, Olympus, Germany) to observe the formation of coacervate/aggregate. The magnification was set at x20. Differential interference contrast (DIC) microscopy images were taken using a LEICA-DMRD microscope equipped with a camera (HAMAMATSU). Observations were carried out on a glass microscope slide with a gene frame (Thermo Scientific).

2.6. Turbidity measurements

Turbidity measurements were carried out by measuring absorbance at 650 nm. Absorbance measurements were conducted using the multicuvette spectrophotometer (UV-1800, Shimadzu, France). Measurements were taken immediately after mixing the biopolymers in different ratios in the 2 mL cuvette (Plastbrand™). Absorbance was converted into turbidity using the equation: $\tau = (2.303 \times A_{650})/l$, where l is the light path length (cm), equal to 1 cm.

2.7. Electrophoretic mobility measurements

Electrophoretic mobility measurements were performed using the Zetasizer nano instrument (Malvern Instruments, UK). Disposable capillary cells (DTS1070) were used for the measurements. 10 runs were conducted for each experiment with an equilibration time of 60 s. All the measurements were repeated three times per sample at 25 °C.

3. Results and discussion

3.1. LYS/ALG complexation proceeds through liquid-solid phase separation at pH 7 and low ionic strength

Positively charged proteins and negatively charged polysaccharides are well known to form complexes through electrostatic interactions. At pH 7, LYS carries a positive charge (0.42 μm cm/V.s mobility), and ALG is negatively charged (−3.814 μm cm/V.s mobility) (Fig. 1A). LYS carries a net positive charge of 8.2 per mol at pH 7 (Kuehner et al., 1999; Spassov & Yan, 2008; Fig. S2 supplementary material). Taking into account the complete protonation at pH 7 for ALG (Haug et al., 1961), the theoretical charge was calculated from the molecular weights of ALG (157 kDa) and the condensed monomer units (176 Da) which give about 892 negative charges per ALG molecule. When mixed, LYS and ALG form turbid solutions instantaneously, which is explained by the formation of aggregates as observed through microscopy (Fig. 1B). This has been observed previously with the same system (Wu, Huang, et al., 2018). However, this is in contrast with the generic assumption that protein/polysaccharide couples mostly form coacervates, especially when weak polyelectrolytes are involved (Kayitmazer, Koksal, & Kilic Iyilik, 2015). Here, ALG is a weak polyelectrolyte and LYS is a weak basic protein, but still, they interact to form aggregates at low ionic strength.

Mixing ratios between the biopolymers drive the charge balance of the system. The turbidity of the LYS/ALG mixture changes with the mixing ratios with maximum turbidity for a LYS:ALG mass ratio of 4:1 at a total polymer concentration of 1 g/L (Fig. 1C). The optimum mixing ratio for complex formation is pH-dependent (Amine, Boire, Kermarrec, & Renard, 2019; Klemmer, Waldner, Stone, Low, & Nickerson, 2012). Under microscopy, samples with higher turbidity present larger connected aggregate structures (Fig. 1B). Electrophoretic mobility measurements have been carried out on the LYS/ALG mixtures at different mixing ratios (Supplementary data, Fig. S1. A). The point where we obtain the maximum turbidity does not show a zero-mobility value, even though it is difficult to interpret the mobility in this context to correlate charge neutrality to zero mobility. According to Anema and de Kruif, a (bio)polymer mixing ratio giving 1:1 charge stoichiometry provides optimum conditions of complex formation as it brings charge neutrality (Anema and de Kruif, 2016). However different results are obtained for the napin/pectin system where coacervation is observed at the point corresponding to the highest charge asymmetry (Amine et al., 2019). The electrophoretic mobility ratio between LYS and ALG, for the same mass of material, measured at pH 7 and low ionic strength, is around 9 (Fig. 1A). This indicates that a given mass of ALG carries about nine times more negative charges than LYS. This suggests that charge neutralization and the highest complex formation should happen at a 9:1 mass ratio of LYS/ALG. The theoretically calculated charge ratios at each mass ratio indicated in Fig. 1C also show the requirement of a mass ratio of 9:1 to reach charge neutrality. However, we here observe the highest turbidity at a ratio of 4:1. This result could be related to the discrepancy between mobility values and effective net charge of each biopolymer and in particular protein (Jachimska, Świątek, Loch, Lewiński, & Luxbacher, 2018) or to counterion-mediated effects due to the presence of salts in the starting materials (Janmey, Slochower, Wang, Wen, & Cēbers, 2014).

3.2. Aggregate formation happens in a wide range of mixing ratios and biopolymer concentrations

The phase behaviour of binary mixtures of biopolymers is known to depend on total concentration and mixing ratio (Amine et al., 2019; Priftis & Tirrell, 2012). Here, we probe the phase behaviour of LYS/ALG mixtures over a wide range of concentrations from 1 to 10 g/L and for 11 mixing ratios. The high viscosity of ALG makes it difficult to work at higher concentrations. The mean grey level of the droplet as a function

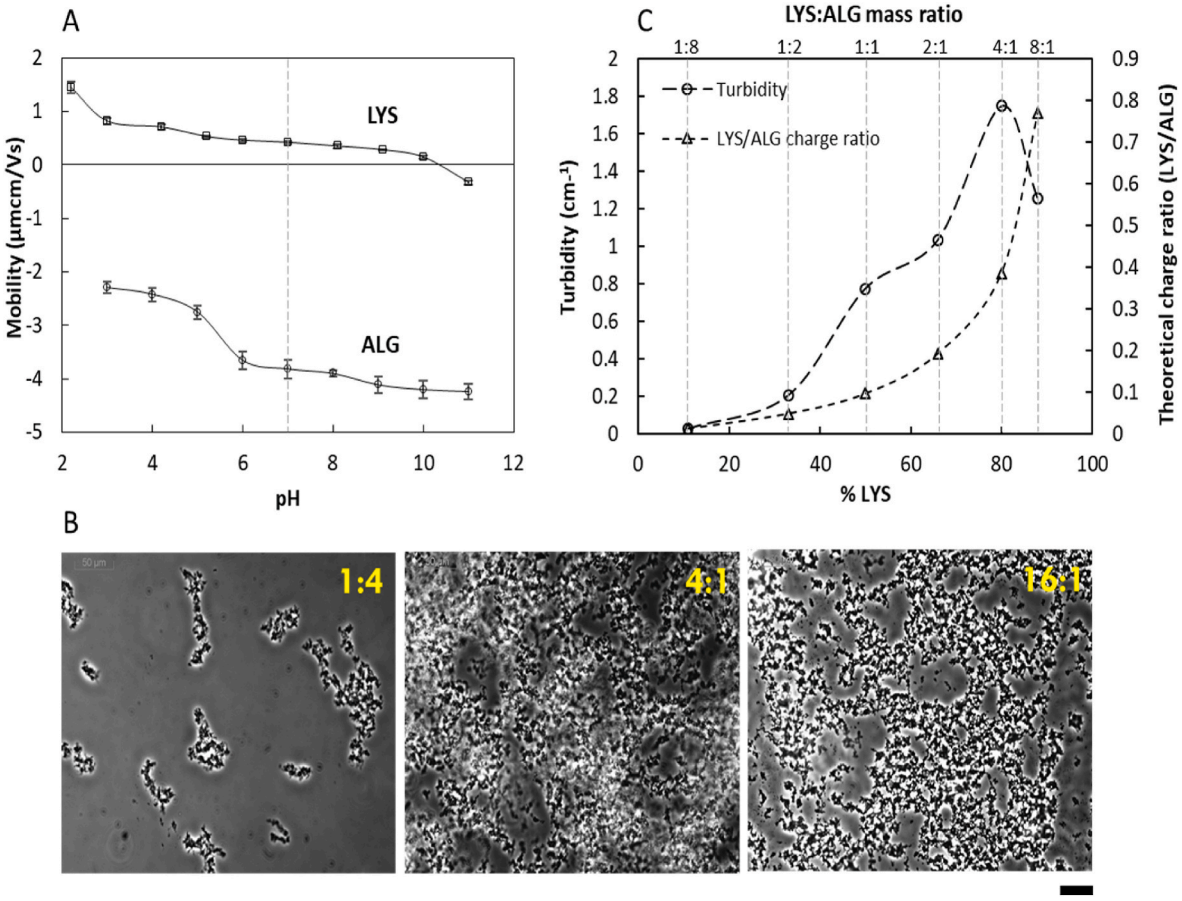

Fig. 1. (A) Electrophoretic mobility values of 2.5 g/L LYS and ALG dispersed in milliQ water at different pHs. (B) Phase contrast microscopy images of LYS/ALG aggregates at three different mixing ratios with a total concentration of 1 g/L (scale bar indicated is 50 μm). (C) Turbidity of the LYS/ALG mixture at different mixing ratios at 1 g/L total concentration in 10 mM HEPES buffer (0 mM NaCl) at pH 7. The mass percentage of LYS in the mixture is indicated in the X-axis. Mass ratios are expressed as LYS:ALG. Theoretically calculated LYS/ALG charge ratios are expressed as the second Y-axis.

of the mixing ratio at 1 g/L follows a trend similar to turbidity (Fig. 1B) with a maximum grey level at the mass ratio 4:1 (Fig. 2A). From the results presented in section 3.1, a threshold mean grey level of 1.8 is found to differentiate conditions for which phase separations occur. This results in a phase diagram comprising homogeneous dispersions (empty squares in Fig. 2B) and phase-separated systems (full squares in Fig. 2B). Even in the presence of a very low ALG concentration, the system phase separates because of the high charge of ALG compared to LYS.

Droplet images at different total concentrations are shown in Fig. 2C. The turbid droplets show heterogeneities even though the proper mixing of the system is validated using TiO_2/water suspensions (supplementary data, Fig. S3). Therefore, the heterogeneous nature of the droplets is associated with aggregation. Moreover, the mean grey level of the droplets increases with increasing the total concentration of biopolymers (Fig. 2D). For the initial mixing ratios, where the grey level is low, there is no real difference in the results across different concentrations. This difference is clearly observable at higher percentages of LYS (from 1:4 to 16:1 LYS/ALG mass ratio) where phase separation is obvious (Fig. 2D). Irrespective of the total biopolymer concentration, phase separation is observed in the same mixing ratios in the total concentrations from 1 g/L to 10 g/L (Fig. 2E). Interestingly, the morphology of the aggregates differs at 10 g/L total concentration, with structures that resemble fibrils (Fig. 2F). This may be linked to the fact that for total concentrations higher than 5 g/L, it is difficult to produce properly separated droplets with the millifluidic device for the intermediate LYS:ALG ratios. In these conditions, solid fiber-like structures are coming out of the capillary, connecting two droplets (droplets corresponding to 10 g/L in Fig. 2C). During the experiment, large complex structures are leaking out of the capillary tube instead of droplets separated by oil. Similar structures appear when the experiments are repeated from high to low levels of ALG and in the reverse. To check if the fibre formation is due to ALG or LYS alone, individual biopolymers at high concentrations (10 g/L) were mixed with buffer, resulting in the absence of the formation of such structures. Hence these structures are confirmed to arise from the mixture of LYS and ALG. At high biopolymer concentrations, these solid filamentous structures form at the T-junction before reaching the capillary, and the oil does not separate them afterward. The shear rate of the system is calculated to be around 5 s^{-1} which is very low and cannot explain the formation of filament. The nature of these filament-like structures and the mechanism of formation remains unknown. These filamentous structures limit us from working with droplet millifluidic in this system at high concentrations (concentrations higher than 5 g/L) and intermediate ratios.

3.3. LYS/ALG complexation proceeds through liquid-liquid phase separation at higher ionic strength

Since the complex formation involves electrostatic interaction, the effect of ionic strength on the phase behaviour of the system was investigated as the presence of salt affects the range and strength of the attractive interactions. Biopolymer dispersions with different concentrations of added salt were prepared and studied using droplet-millifluidics. For a total biopolymer concentration of 5 g/L, the mean grey level first increases until 125 mM NaCl; and then decreases after 125 mM NaCl (Fig. 3A). After 175 mM, the mixture finally appears translucent. The droplets look less heterogeneous as the salt

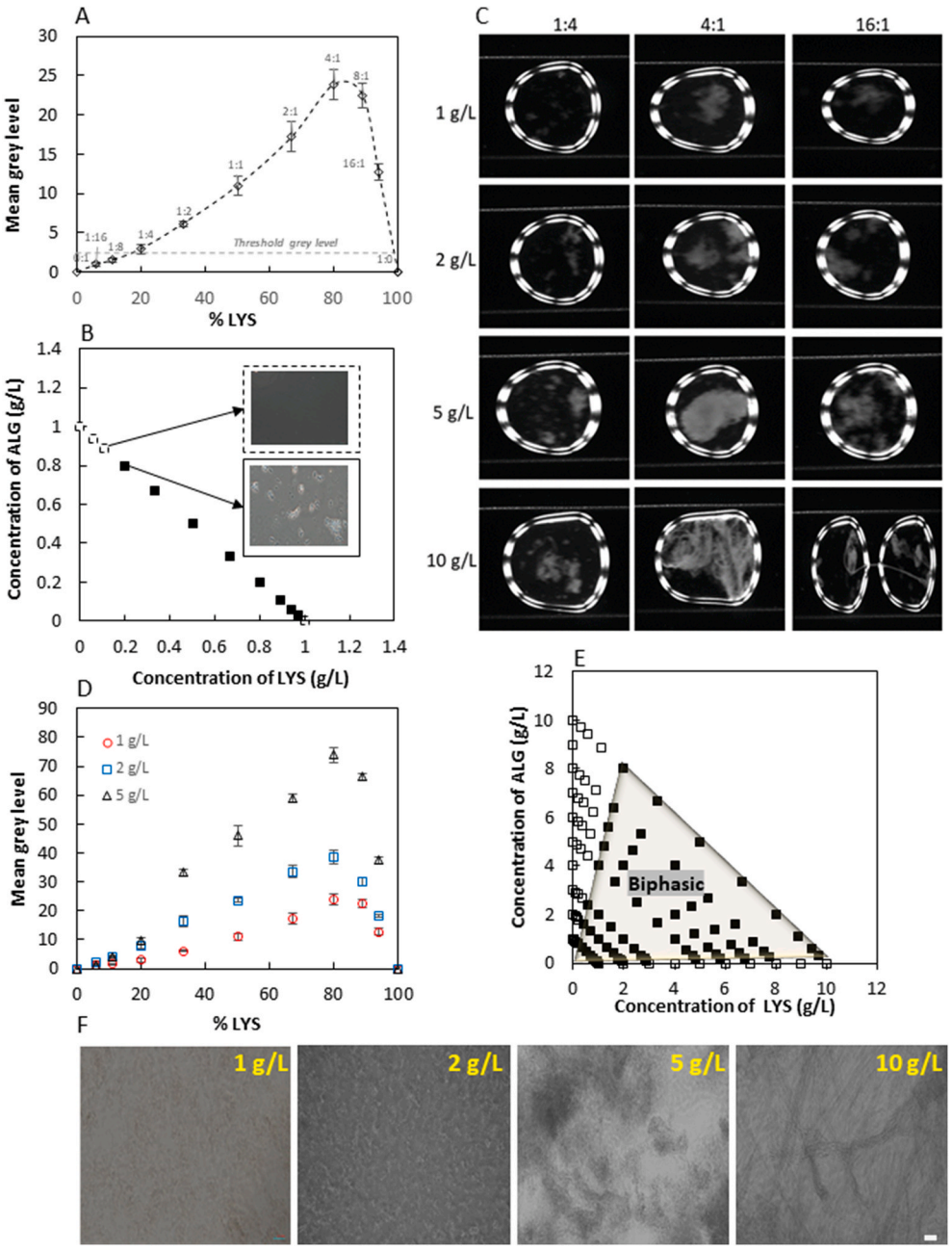

Fig. 2. (A) Mean grey level values of LYS/ALG mixtures at different mixing ratios obtained from droplet-millifluidic experiment for a total concentration of 1 g/L (10 mM HEPES buffer, pH 7). The mean grey level value is at its maximum for the mixture at ratio 4:1 (B) Millifluidic phase diagram of LYS/ALG mixture for a total concentration of 1 g/L. Phase separation starts for a ratio of 1:4 and the system exists in the biphasic region even at low ALG concentration (C) Droplet images of 1 g/L, 2 g/L, 5 g/L, and 10 g/L total concentrations of LYS/ALG mixtures at pH 7 (10 mM HEPES buffer) and three mixing ratios. The grey level developed inside the droplet increases with the total biopolymer concentration. At 10 g/L total concentration, fibril-like structures appear in the millifluidic device. (D) Mean grey level values at three total concentrations and different mixing ratios. (E) Phase diagram of LYS/ALG delimiting the biphasic from the monophasic regions. In all total concentrations, phase separation is observed in the same range of mixing ratios. (F) Phase contrast microscopy images of LYS:ALG at a ratio of 4:1 in 1 g/L, 2 g/L, 5 g/L, and 10 g/L total concentrations.

concentration increases. The grey level distribution inside the droplets was obtained using image J. At different ionic strengths, the grey level intensities normalized with the number of pixels inside the selected area are shown in Fig. 3C. When these mixtures are observed under microscopy, the complex morphology changes from aggregates to coacervates as we go from low to high ionic strengths (Fig. 3B). The coacervate microdroplets are tiny round structures that are dynamic in nature but do not coalesce when observed under phase contrast microscopy. At low biopolymer concentrations, they are even smaller in size and difficult to probe with light microscopy. The differential interference contrast (DIC) images of structures obtained at different salt concentrations and fixed mass ratio 8:1 are shown in Fig. S4 (supplementary data). In bulk, the coacervates are stable over time and a complete macroscopic LLPS is very slow (Fig. S5 in supplementary data). A phase where both solid and liquid phases coexist is observed as well at 100 mM NaCl. The coexistence of different phases is also demonstrated in the gelatin-maltodextrin biopolymeric couple where authors identify three equilibrium phases (Masullo et al., 2020). Bringing down the interaction strength between biopolymers by screening charges causes coacervation whereas, at low salt conditions, high interaction between the

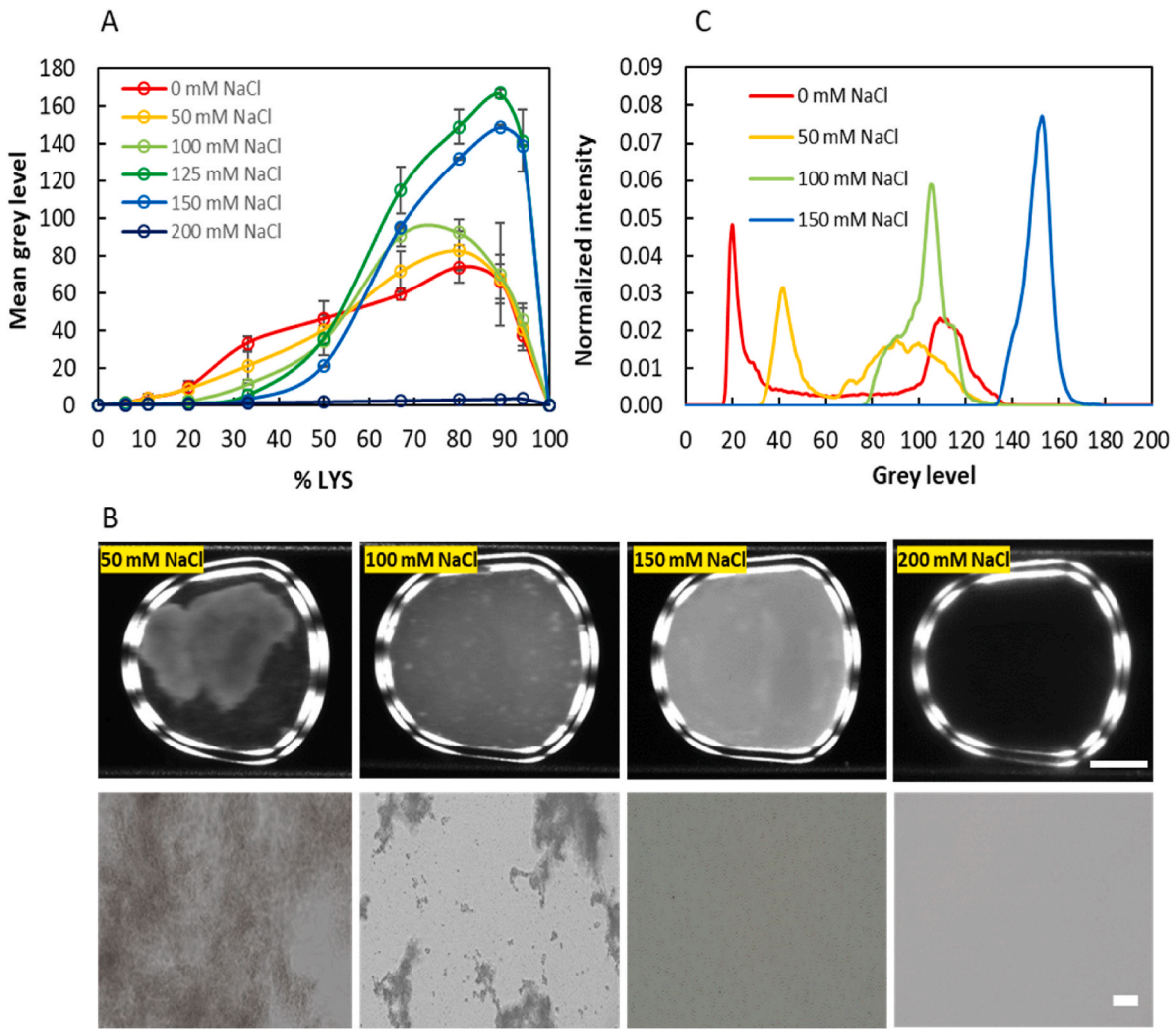

Fig. 3. (A) Mean grey levels of LYS-ALG mixtures at 5 g/L total polymer concentration and different mixing ratios at pH 7 in different ionic strengths. The mean grey level at higher LYS:ALG ratios increases as the ionic strength increases till 125 mM and, beyond that, the grey level decreases and reaches zero at 200 mM NaCl (B) Droplet images of 5 g/L total concentration and 8:1 ratio with different ionic strengths (scale bar is 0.5 mm) and phase contrast microscopy images of LYS:ALG mixture with a total concentration of 5 g/L and mixing ratio of 8:1 in different ionic strengths (scale bar is 50 μm). (C) Grey-level histograms of 5 g/L LYS:ALG mixtures at different ionic strengths.

biopolymers leads to aggregate formation. The transition of solid polyelectrolyte complex to liquid complex coacervates in the presence of added KBr has been observed in the system containing poly (4-styrene sulfonic acid, sodium salt) (PSS) and poly (diallyl dimethyl ammonium chloride) (PDADMAC) (Liu, Momani, et al., 2017). According to them, decreased salt concentration leads to the formation of trapped electrostatic crosslinks leading to the formation of solid aggregates. The electrophoretic mobility measurements have been carried out on LYS and ALG at 5 g/L concentration and different ionic strengths, but the instrument failed to give a mobility distribution plot or the proper raw data at higher ionic strengths as the conductivity of the solution was above 5 mS/cm at high ionic strengths. Mobility of ALG became less negative till 50 mM NaCl and above that reliable data were not obtained. The mobility value of LYS decreases till 50 mM NaCl. At higher ionic strengths, the instrument gave negative mobility values (data not shown). That could be due to the anionic-specific adsorption of chloride anions onto the surface of the protein (Henry et al., 2017; T et al., 1950). The fact that ALG and LYS interact on the wrong side at high ionic strength leading to coacervation could be explained by the presence of positive patches at the LYS surface (see Fig. 3D in Henry et al., 2017).

The homogenous appearance of the droplets is associated with the formation of coacervate microdroplets at higher ionic strength whereas at low ionic strength, the aggregates formed give rise to heterogeneous droplets. A striking result is the non-monotonous decrease of turbidity with increasing salt concentration for LYS:ALG mass ratios comprised between 2:1 and 16:1. As the concentration of NaCl increases in the mixture, the turbidity is expected to decrease due to the decrease in the range of interaction, as observed for polyelectrolyte complexes (Perry, Li, Priftis, Leon, & Tirrell, 2014). Instead, we observe an increase of the mean grey value from 0 to 125 mM added NaCl, and the expected decrease for larger ionic strength. The histograms in Fig. 3C show a bimodal distribution of the grey level for ionic strength below 50 mM. The calculated mean grey value is therefore lower than the grey level of the dense phases. Still, the mean grey population of the lighter part is lower than the mean grey value obtained at 100 and 150 mM. This unexpected change in grey level with increasing salt concentration may be due to a change in the number, size, and/or density of the dense phases generated by the phase separation. Anyhow, the change in the mean grey level values with the increased salt concentration is associated with the change of assembly from aggregation to coacervation. The volume fraction of the complexes formed at different ionic strengths and the LYS:ALG mass ratio of 8:1 were checked in the bulk. The bulk experiment did not support the trend in the grey level where the volume fraction of the dense phase appeared to be higher at 0 mM NaCl (Fig. S5

in supplementary data). The tendency of the coacervate droplets to be stable over time also prevents us from comparing the volume fraction of the dense phases at different ionic strengths. In Fig. 3A, we can also see that, in the lower LYS:ALG ratios, mean grey levels are decreasing with increasing salt concentration. LYS is more affected by salt as compared to ALG. When we have a lesser LYS concentration in the mixture, the charges on LYS are screened by the added salt causing no or reduced complex formation. Total biopolymer concentrations ranging from 1 g/L to 10 g/L were probed with salt concentrations up to 200 mM and similar results were observed in all concentration conditions (data not shown).

3.4. Differentiating aggregation and coacervation

Interestingly, the level of homogeneity of droplet images indicates the type of phase separation: homogenous grey level distribution is associated with coacervation and heterogeneous grey level distribution to aggregation (Fig. 3C). We intend to use this difference in grey level distribution as an indicator of the type of phase separation. For a droplet with a homogeneous, well-distributed grey level, the grey level distribution curve is symmetric and narrow, with a mean grey level value close to the median grey level value. In contrast, in the case of aggregation, we have heterogeneous droplets where the grey level is not well distributed throughout the droplet. In Fig. 3C, at 0 mM NaCl and 50 mM NaCl, we have two broad peaks. In that case, the mean and median grey levels differ a lot. At the NaCl concentration of 100 mM, where we observe the coexistence of two states, the complexes are distributed all over the droplets, yet we have white spots at different grey levels. At 150 mM NaCl, we have a narrow grey level distribution curve with close mean and median values. Table S2 (supplementary data) summarizes the differentiation made between aggregation and coacervation by the grey level analysis. In the case of homogeneous coacervates, the difference between mean and median grey level values is less than 1%. A higher disparity between the mean and median values is obtained for

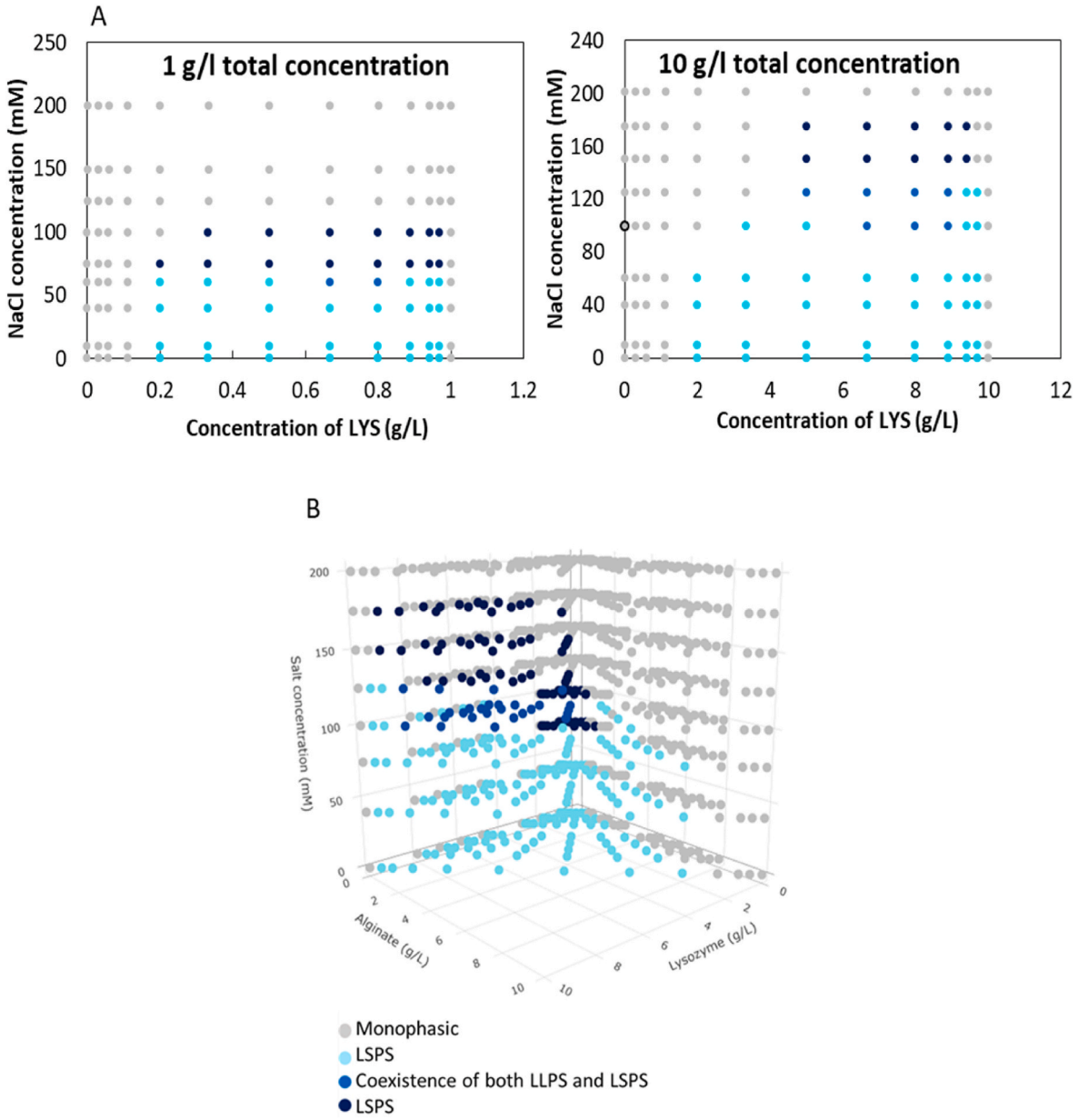

Fig. 4. (A) LYS/ALG phase diagram of 1 g/L and 10 g/L total concentrations in different salt conditions at pH 7. (B) 3D phase diagram of LYS/ALG with total polymer concentrations ranging from 1 g/L to 10 g/L and added salt concentrations from 0 to 200 mM NaCl. LSPS: liquid-solid phase separation; LLPS: liquid-liquid phase separation.

aggregates which is more evident at lower biopolymer concentrations. The change for aggregates is very high, i.e. 55 %, at low biopolymer concentrations. As the total concentration of the biopolymer is higher, the change is less obvious for aggregates. When the biopolymer concentrations are low, we have a lesser number of charges available for interacting and we obtain low complex formation. Because of the heterogeneous distribution of the solid structures formed, we have more black area inside the droplet while there are more structures occupying the area of the droplets at high concentrations. A much evident discrepancy between mean and median values is therefore observed in the droplets corresponding to aggregation at lower biopolymer concentrations like 1 g/L. However, under all conditions, a value less than or equal to 1% is observed for coacervates irrespective of the total polymer concentration. However, this method of differentiating aggregation and coacervation is quite specific to this couple of biopolymers. All systems might not necessarily be following this trend of grey level distribution. We cannot talk about the underlying mechanism of the different phase separation pathways from the grey level analysis. However, we can still make assumptions, such as suggesting that strong interactions may lead to the formation of densely distributed structures (aggregates) with a high refractive index. To establish a broader understanding of linking complex formation to grey levels, it's essential to examine the phase behaviour and trends in grey level distribution among different interacting couples.

3.5. Different phase boundaries for different biopolymer concentration

In section 3.2, we have seen that aggregation occurs at all concentrations in the same mixing ratios at low ionic strength. But when salt is added, the effect of ionic strength is not the same at different biopolymer concentrations. The phase diagrams for the total concentrations of 1 g/L and 10 g/L at different ionic strengths are shown in Fig. 4A. When the total biopolymer concentration is 10 g/L, phase separation occurs even at 175 mM ionic strength and ceases at 200 mM when compared to lower concentrations like 1 g/L, which takes place only until 125 mM salt concentration. At higher biopolymer concentrations, more salt is required to suppress the complex formation. At 1 g/L total concentration, coacervation occurs at 75 mM salt concentration, but 150 mM salt is needed to have coacervation when the total concentration is 10 g/L. When the biopolymer concentration is high, more charged sites are available. The amount of salt required to screen the charges and reduce the interaction will therefore clearly differ based on the biopolymer concentration.

As we go to higher ionic strength at a given total biopolymer concentration, more LYS is needed to have phase separation (Fig. S6, supplementary data). Different ionic strengths and total concentrations define the biphasic region differently. So, the different propensity of the two components to phase separate can be shown using a 3D phase diagram by taking ionic strength and total concentration as the control variables (Fig. 4B). The grey colour dots represent the region where the system exists in the monophasic region. The cyan colour dots show the area where we observed liquid-solid phase separation forming aggregates whereas coacervated forming conditions are shown by navy blue coloured points. In between we also have a region where both liquid and solid structures coexist, represented by dark blue dots. We can see here that increasing ionic strength narrows the phase separation domain.

3.6. Tight binding between the biopolymers leads to aggregation while coacervation is associated with a lower affinity

From the millifluidic experiments, we see different conditions of salt concentration leading to aggregated and coacervated states. It is interesting to see how the thermodynamic parameters associated with the binding events of the complex formation change based on the different ionic strengths of the mixture. The thermodynamic characterization of LYS-ALG complex formation was carried out using a VP-ITC microcalorimeter. Based on the phase diagram, two conditions of ionic strengths were chosen for a total biopolymer concentration coming around 1 g/L, corresponding to aggregation (0 NaCl) and complex coacervation (75 mM NaCl), respectively. LYS was taken in the cell and titrated with ALG since excess LYS concentration was needed in the mixture.

The results are shown in Fig. 5. For the lowest ionic strength conditions, we have a sudden upturn in the thermogram. The complex formation is clearly visible and the heat effect caused by this process is much larger than the respective heat of dilution. The transition point (N) occurs at a molar ratio of 0.01 indicating a stoichiometry of 100 LYS molecules per ALG unit, which is about the theoretically calculated charge stoichiometry (supplementary data, Table s1). The rectangular-shaped curve of the thermogram corresponds to the strong affinity between LYS and ALG. Given the recovered strong interaction between LYS and ALG, 5–6 titration experiments at different concentrations of LYS and/or ALG were carried out to reach an exploitable shape of the binding isotherms. This was achieved using the classic ITC equation, $c = K_{a*}M_{tot*}N$, linking the concentration of the macromolecule in the cell (M_{tot}) to the affinity constant (K_a) and stoichiometry (N) of the interaction (Perozzo, Folkers, & Scapozza, 2004). The shape of the thermogram and the molar ratio at which transition occurs, point N, are insensitive to the decrease of the concentration of both biopolymers during titration experiments (supplementary data, Fig. S7). The achievement of charge neutrality at the stoichiometry condition is confirmed using electrophoretic mobility measurements where we got a zero-mobility value for the same ratio (supplementary data, Fig. S8). For low and high salt concentrations, the data can be fitted by a single set of independent binding sites model. The calculated apparent affinity constant K_a between LYS and ALG was found to be ≈ August 2, 10^{10} M^{-1}. Increasing the ionic strength to 75 mM strongly decreases the binding affinity, with a 500-fold decrease in the calculated apparent K_a value to $\approx 6.0.10^7$ M^{-1}, without any significant change in the stoichiometry point N. When we compare with the values of K_a obtained for coacervates of previous works, still the value is high. The microscopy observations confirm the presence of coacervates at this higher ionic strength (data not shown).

The thermodynamic insight obtained from ITC primarily shows that the interacting process is exothermic (negative enthalpy) at both ionic strengths. Negative enthalpy (ΔH) values of $-8.4.10^5$ $J.mol^{-1}$ and $-6.9.10^5$ $J.mol^{-1}$ are obtained at lower and higher ionic strengths respectively. Entropy values (ΔS) obtained in both conditions are also negative ($-2.7.10^3$ $J.K^{-1}.mol.^{-1}$ at low ionic strength and $-2.3.10^3$ $J.K^{-1}.mol.^{-1}$ at higher ionic strength). This suggests that the interaction and self-assembly process is driven enthalpically, corresponding to an electrostatic interaction in which the negative entropy reflects the structural fixation of the interacting molecules.

From the literature data, the enthalpy-driven process is related to the energy involved in molecular interactions and reflects the contribution of hydrogen bonds, electrostatic interactions, and van der Waals forces (Saboury, 2003). More generally, in the case of weakly charged polyelectrolytes, the complex formation is associated with negative enthalpy ΔH due to electrostatic attraction, with counterion release entropy playing only a minor role (Turgeon et al., 2007). The interaction of LYS and ALG at pH 4.5 was also reported to be exothermic (Fuenzalida et al., 2016; Wu, Huang, et al., 2018). At low salt conditions, the affinity between LYS and ALG at pH 7 is very high, therefore leading to a rectangular-shaped isotherm with a sharp increase in energy happening at the stoichiometric equivalent point N. This kind of steep thermogram is not common in protein-polysaccharide interactions. The steep increase in the ITC curve is characteristic of a very strong affinity between biopolymers leading to aggregation. Similar curves have been previously observed for the aggregation of the surfactant zwitterionic sulfobetaine SB3-12 with an alkyl chain (Loh, Brinatti, & Tam, 2016) and LYS complexation to heparin (Malicka, Haag, & Ballauff, 2022). Usually, ITC is best suited to interaction strengths with a value of an apparent K_a no

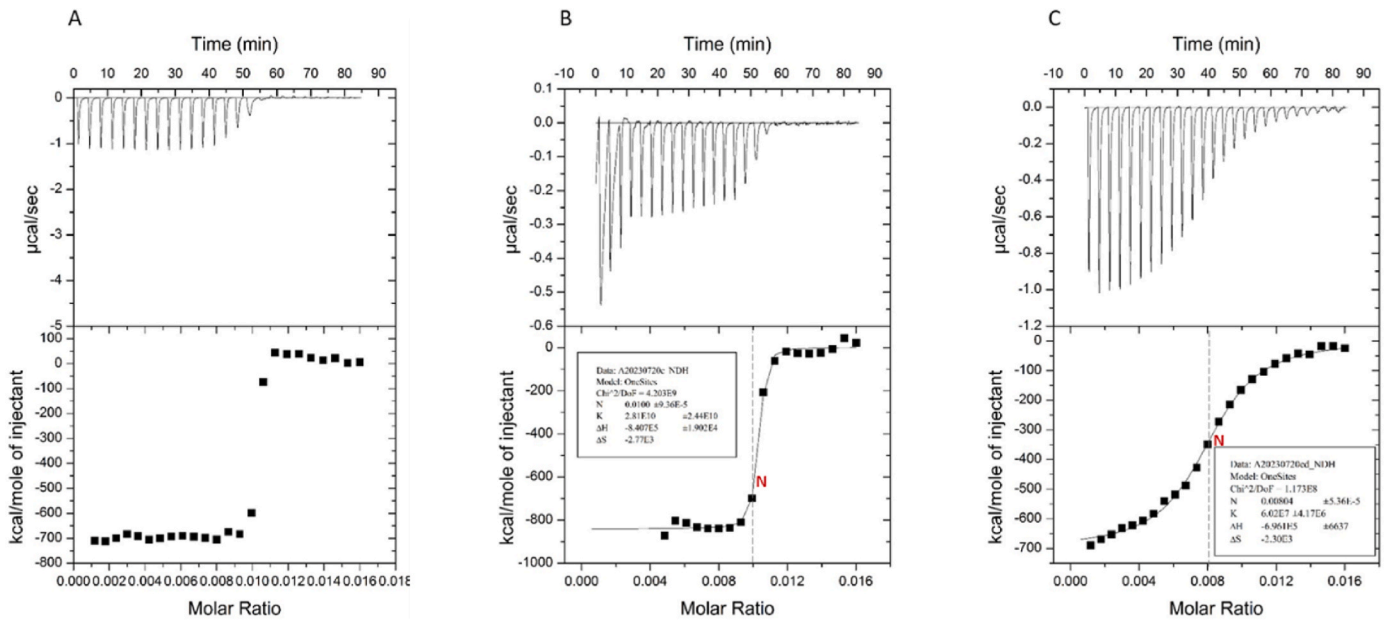

Fig. 5. ITC thermograms obtained at 25 °C by injecting (A) 0.94 μM ALG into 11.2 μM LYS without added NaCl, and (B) 4.7 μM ALG into 56 μM LYS in the presence of 75 mM NaCl. The thermogram given in A corresponds to aggregation and B corresponds to coacervation. All the solutions were prepared in 10 mM HEPES buffer at pH 7. The upper panel shows the heat flow thermogram as a function of time obtained during the titration of LYS by ALG and the bottom panel is the integrated data of enthalpy versus ALG:LYS molar ratio.

more than 1 nM^{-1}. For the LYS-ALG mixture at low ionic strength, an apparent K_a of 2.8 10^{10} M^{-1} is calculated which is very high. Nevertheless, considering the huge difference in charge number between LYS and ALG molecules at pH 7 (≈100), the value of K_a, expressed based on charge ratio, decreases to the reasonable value of ≈2.8 10^8 M^{-1}. We could bring down the binding affinity between the two biopolymers to 6.0.10^7 M^{-1} (≈6.0 10^5 M^{-1}) by adding salt and thus reorganizing the assembly towards coacervation.

From ITC experiments, the stoichiometry value N is found to be reached at ALG:LYS molar ratio of 0.01 corresponding to 100 molecules of LYS per ALG. From the theoretical calculation of available charges on both LYS and ALG molecules, as indicated above, a hundred units of LYS are required for one ALG to acquire charge neutrality. Even though all the charges on both biopolymers might not be available for interaction, the experimentally observed stoichiometry is consistent with the theoretically obtained stoichiometry. The salt concentration-dependent strength of the initial interaction between the two biopolymers drives the nature of the final phase separation, liquid-solid (aggregates) versus liquid-liquid (coacervates) at low and high ionic strength, respectively.

4. Conclusions

The formation of LYS and ALG complexes in different conditions of mixing ratio, total polymer concentration, and ionic strength are investigated using droplets-based millifluidic, turbidity, and microscopy. The droplet-based millifluidic device coupled with optical microscopy gives us an extensive qualitative analysis of the phase behaviour of the system by probing different conditions of mixing. Similar results are obtained from grey level analyses and turbidity measurements conducted in bulk. The level analysis method is an easy way of checking phase separation and having a qualitative idea of complex formation under different tested conditions by looking at the homogeneity in the droplets. The homogenous appearance of the droplets is associated with the formation of coacervate microdroplets at higher ionic strength whereas at low ionic strength, the aggregates formed give rise to heterogeneous droplets. Therefore, a quantitative assessment by comparing the mean and median grey level values gives us a way to distinguish between aggregates and coacervates. It is not possible, however, to use droplet-based millifluidics to investigate phase separation at its earliest stage.

We tune the interaction strength between LYS and ALG by the addition of NaCl, and depending on the salt concentrations we observe regions where the system exists as soluble complexes, aggregates, and coacervates; with sometimes the coexistence of both solid and liquid structures. For the first time to our knowledge, using droplets-based millifluidic, four physical states are identified: homogeneous liquid (i.e. monophasic), liquid-solid (i.e. aggregation), liquid-liquid (i.e. coacervation) and coexistence of liquid-solid and liquid-liquid. Thermodynamic characterization of the aggregation and coacervation phenomena is carried out using ITC. ITC data clearly show the requirement of strong affinity for aggregation and reduced affinity to have coacervation in the LYS-ALG mixture. These are important results that give crucial information about the mechanisms involved in the coacervation/aggregation of protein/polysaccharide systems. However, the driving force for coacervation or aggregation depends on the system studied, especially on features like the charge density and flexibility of the polysaccharide, and the charge distributions of the protein. For better rationalizing the two LSPS and LLPS processes, other polyelectrolyte couples need to be investigated to unravel the mechanisms underlying the two phase separation processes.

CRediT authorship contribution statement

Asna Vakeri: Writing – review & editing, Writing – original draft, Investigation, Formal analysis, Conceptualization. **Adeline Boire:** Writing – review & editing, Supervision, Resources, Conceptualization. **Joelle Davy:** Methodology. **Pascaline Hamon:** Methodology. **Antoine Bouchoux:** Writing – review & editing, Conceptualization. **Saïd Bouhallab:** Writing – review & editing, Supervision, Resources, Conceptualization. **Denis Renard:** Writing – review & editing, Supervision, Resources, Funding acquisition, Conceptualization.

Declaration of competing interest

The authors declare that they have no known competing financial interests or personal relationships that could have appeared to influence

the work reported in this paper.

Data availability

Data will be made available on request.

Acknowledgments

The authors acknowledge Anne-Laure Reguerre for helping with the image analysis. This work was carried out with the financial support of the National Research Institute for Agriculture, Food and the Environment (INRAE) and Région Pays de la Loire.

Appendix A. Supplementary data

Supplementary data to this article can be found online at https://doi.org/10.1016/j.foodhyd.2024.110359.

References

Ainis, W. N., Boire, A., Solé-Jamault, V., Nicolas, A., Bouhallab, S., & Ipsen, R. (2019). Contrasting assemblies of oppositely charged proteins. *Langmuir, 35*(30), 9923–9933. https://doi.org/10.1021/acs.langmuir.9b01046

Amine, C., Boire, A., Davy, J., Marquis, M., & Renard, D. (2017). Droplets-based millifluidic for the rapid determination of biopolymers phase diagrams. *Food Hydrocolloids, 70*, 134–142. https://doi.org/10.1016/j.foodhyd.2017.03.035

Amine, C., Boire, A., Davy, J., Reguerre, A. L., Papineau, P., & Renard, D. (2020). Optimization of a droplet-based millifluidic device to investigate the phase behavior of biopolymers, including viscous conditions. *Food Biophysics, 15*(4), 463–472. https://doi.org/10.1007/s11483-020-09645-9

Amine, C., Boire, A., Kermarrec, A., & Renard, D. (2019). Associative properties of rapeseed napin and pectin: Competition between liquid-liquid and liquid-solid phase separation. *Food Hydrocolloids, 92*(December 2018), 94–103. https://doi.org/10.1016/j.foodhyd.2019.01.026

Anema, S. G., & Kees de Kruif, C. G. (2016). Phase separation and composition of coacervates of lactoferrin and caseins. *Food Hydrocolloids, 52*, 670–677. https://doi.org/10.1016/j.foodhyd.2015.08.011

Blocher, W. C., & Perry, S. L. (2017). Complex coacervate-based materials for biomedicine. *Wiley Interdisciplinary Reviews: Nanomedicine and Nanobiotechnology, 9*(4), 76–78. https://doi.org/10.1002/wnan.1442

Comert, F., Malanowski, A. J., Azarikia, F., & Dubin, P. L. (2016). Coacervation and precipitation in polysaccharide-protein systems. *Soft Matter, 12*(18), 4154–4161. https://doi.org/10.1039/c6sm00044d

Fuenzalida, J. P., Nareddy, P. K., Moreno-Villoslada, I., Moerschbacher, B. M., Swamy, M. J., Pan, S., et al. (2016). On the role of alginate structure in complexing with lysozyme and application for enzyme delivery. *Food Hydrocolloids, 53*, 239–248. https://doi.org/10.1016/j.foodhyd.2015.04.017

Ghosh, B., Bose, R., & Tang, T. Y. D. (2021). Can coacervation unify disparate hypotheses in the origin of cellular life? *Current Opinion in Colloid & Interface Science, 52*, Article 101415. https://doi.org/10.1016/j.cocis.2020.101415

Harnsilawat, T., Pongsawatmanit, R., & McClements, D. J. (2006). Characterization of β-lactoglobulin-sodium alginate interactions in aqueous solutions: A calorimetry, light scattering, electrophoretic mobility and solubility study. *Food Hydrocolloids, 20*(5), 577–585. https://doi.org/10.1016/j.foodhyd.2005.05.005

Haug, A., Rasmussen, S. E., Sheppard, R. C., Terry, W. G., Sjöberg, B., & Toft, J. (1961). Dissociation of alginic acid. *Acta Chemica Scandinavica, 15*, 950–952. https://doi.org/10.3891/acta.chem.scand.15-0950

Henry, N., Clouet, J., Le Visage, C., Weiss, P., Gautron, E., Renard, D., et al. (2017). Silica nanofibers as a new drug delivery system: A study of the protein-silica interactions. *Journal of Materials Chemistry B, 5*(16), 2908–2920. https://doi.org/10.1039/c7tb00332c

Jachimska, B., Świątek, S., Loch, J. I., Lewiński, K., & Luxbacher, T. (2018). Adsorption effectiveness of β-lactoglobulin onto gold surface determined by quartz crystal microbalance. *Bioelectrochemistry, 121*, 95–104. https://doi.org/10.1016/j.bioelechem.2018.01.010

Janmey, P. A., Slochower, D. R., Wang, Y. H., Wen, Q., & Cēbers, A. (2014). Polyelectrolyte properties of filamentous biopolymers and their consequences in biological fluids. *Soft Matter, 10*(10), 1439–1449.

Kayitmazer, A. B., Koksal, A. F., & Kilic Iyilik, E. (2015). Complex coacervation of hyaluronic acid and chitosan: Effects of pH, ionic strength, charge density, chain length and the charge ratio. *Soft Matter, 11*(44), 8605–8612. https://doi.org/10.1039/c5sm01829c

Klemmer, K. J., Waldner, L., Stone, A., Low, N. H., & Nickerson, M. T. (2012). Complex coacervation of pea protein isolate and alginate polysaccharides. *Food Chemistry, 130*(3), 710–715. https://doi.org/10.1016/j.foodchem.2011.07.114

Kuehner, D. E., Engmann, J., Fergg, F., Wernick, M., Blanch, H. W., & Prausnitz, J. M. (1999). Lysozyme net charge and ion binding in concentrated aqueous electrolyte solutions. *Journal of Physical Chemistry B, 103*(8), 1368–1374. https://doi.org/10.1021/jp983852i

Kurut, A., Persson, B. A., Åkesson, T., Forsman, J., & Lund, M. (2012). Anisotropic interactions in protein mixtures: Self assembly and phase behavior in aqueous solution. *Journal of Physical Chemistry Letters, 3*(6), 731–734. https://doi.org/10.1021/jz201680m

Liu, Y., Momani, B., Winter, H. H., & Perry, S. L. (2017). Rheological characterization of liquid-to-solid transitions in bulk polyelectrolyte complexes. *Soft Matter, 13*(40), 7332–7340. https://doi.org/10.1039/c7sm01285c

Loh, W., Brinatti, C., & Tam, K. C. (2016). Use of isothermal titration calorimetry to study surfactant aggregation in colloidal systems. *Biochimica et Biophysica Acta - General Subjects, 1860*(5), 999–1016. https://doi.org/10.1016/j.bbagen.2015.10.003

Malicka, W., Haag, R., & Ballauff, M. (2022). Interaction of heparin with proteins: Hydration effects. *Journal of Physical Chemistry B, 126*(33), 6250–6260. https://doi.org/10.1021/acs.jpcb.2c04928

Masullo, F., Beldengrün, Y., Miras, J., Mackie, A. D., Esquena, J., & Avalos, J. B. (2020). Phase behavior of gelatin/maltodextrin aqueous mixtures studied from a combined experimental and theoretical approach. *Fluid Phase Equilibria, 524*. https://doi.org/10.1016/j.fluid.2020.112675

Nigen, M., Croguennec, T., Renard, D., & Bouhallab, S. (2007). Temperature affects the supramolecular structures resulting from α-lactalbumin - lysozyme interaction. *Biochemistry, 46*(5), 1248–1255. https://doi.org/10.1021/bi062129c

Pathak, J., Priyadarshini, E., Rawat, K., & Bohidar, H. B. (2017). Complex coacervation in charge complementary biopolymers: Electrostatic versus surface patch binding. *Advances in Colloid and Interface Science, 250*, 40–53. https://doi.org/10.1016/j.cis.2017.10.006

Perozzo, R., Folkers, G., & Scapozza, L. (2004). Thermodynamics of protein-ligand interactions: History, presence, and future aspects. *Journal of Receptors and Signal Transduction, 24*(1–2), 1–52. https://doi.org/10.1081/RRS-120037896

Perry, S. L., Leon, L., Hoffmann, K. Q., Kade, M. J., Priftis, D., Black, K. A., et al. (2015). Chirality-selected phase behaviour in ionic polypeptide complexes. *Nature Communications, 6*. https://doi.org/10.1038/ncomms7052

Perry, S. L., Li, Y., Priftis, D., Leon, L., & Tirrell, M. (2014). The effect of salt on the complex coacervation of vinyl polyelectrolytes. *Polymers, 6*(6), 1756–1772. https://doi.org/10.3390/polym6061756

Persson, B. A., & Lund, M. (2009). Association and electrostatic steering of α-lactalbumin-lysozyme heterodimers. *Physical Chemistry Chemical Physics, 11*(39), 8879–8885. https://doi.org/10.1039/b909179c

Priftis, D., & Tirrell, M. (2012). Phase behaviour and complex coacervation of aqueous polypeptide solutions. *Soft Matter, 8*(36), 9396–9405. https://doi.org/10.1039/c2sm25604e

Romanini, D., Braia, M., Angarten, R. G., Loh, W., & Picó, G. (2007). Interaction of lysozyme with negatively charged flexible chain polymers. *Journal of Chromatography, B: Analytical Technologies in the Biomedical and Life Sciences, 857*(1), 25–31. https://doi.org/10.1016/j.jchromb.2007.06.025

Saboury, A. A. (2003). Application of a new method for data analysis of isothermal titration calorimetry in the interaction between human serum albumin and Ni2+. *Journal of Chemical Thermodynamics, 35*(12), 1975–1981. https://doi.org/10.1016/j.jct.2003.08.006

Schmidt, I., Cousin, F., Huchon, C., Boué, F., & Axelos, M. A. V. (2009). Spatial structure and composition of polysaccharide-protein complexes from small angle neutron scattering. *Biomacromolecules, 10*(6), 1346–1357. https://doi.org/10.1021/bm801147j

Schmitt, C., & Turgeon, S. L. (2011). Protein/polysaccharide complexes and coacervates in food systems. *Advances in Colloid and Interface Science, 167*(1–2), 63–70. https://doi.org/10.1016/j.cis.2010.10.001

Sinha, N. J., Cunha, K. C., Murphy, R., Hawker, C. J., Shea, J. E., & Helgeson, M. E. (2023). Competition between β-sheet and coacervate domains yields diverse morphologies in mixtures of oppositely charged homochiral polypeptides. *Biomacromolecules, 24*(8), 3580–3588. https://doi.org/10.1021/acs.biomac.3c00361

Spassov, V. Z., & Yan, L. (2008). A fast and accurate computational approach to protein ionization. *Protein Science, 17*(11), 1955–1970. https://doi.org/10.1110/ps.036335.108

Sun, X., Xiao, J. X., & Huang, G. Q. (2019). Recovery of lysozyme from aqueous solution by polyelectrolyte precipitation with sodium alginate. *Food Hydrocolloids, 90*(June 2018), 225–231. https://doi.org/10.1016/j.foodhyd.2018.12.024

T, B. J., Edelhoch, H., Lontie, R., Morrison, P. R., Edeliioch, H., & Lontie, R. (1950). *Edge generous financial support by the Research Light Scattering in Solutions of Serum Albumin : Effects of Charge and Ionic containing two or more proteins , which may inter-, 467*, 5.

Turgeon, S. L., Schmitt, C., & Sanchez, C. (2007). Protein – polysaccharide complexes and coacervates. *Current Opinion in Colloid & Interface Science, 12*, 166–178. https://doi.org/10.1016/j.cocis.2007.07.007

Wu, T., Huang, J., Jiang, Y., Hu, Y., Ye, X., Liu, D., et al. (2018). Formation of hydrogels based on chitosan/alginate for the delivery of lysozyme and their antibacterial activity. *Food Chemistry, 240*, 361–369. https://doi.org/10.1016/j.foodchem.2017.07.052

Wu, T., Li, Y., Shen, N., Yuan, C., & Hu, Y. (2018). Preparation and characterization of calcium alginate-chitosan complexes loaded with lysozyme. *Journal of Food Engineering, 233*, 109–116. https://doi.org/10.1016/j.jfoodeng.2018.03.020

Xu, A. Y., Melton, L. D., Ryan, T. M., Mata, J. P., Rekas, A., Williams, M. A. K., et al. (2018). Effects of polysaccharide charge pattern on the microstructures of β-lactoglobulin-pectin complex coacervates, studied by SAXS and SANS. *Food Hydrocolloids, 77*, 952–963. https://doi.org/10.1016/j.foodhyd.2017.11.045

Zheng, J., Gao, Q., Ge, G., Wu, J., Tang, C. he, Zhao, M., et al. (2022). Dynamic equilibrium of β-conglycinin/lysozyme heteroprotein complex coacervates. *Food Hydrocolloids, 124*(October 2021). https://doi.org/10.1016/j.foodhyd.2021.107339